Inorg. Chem. **2009**, *48*, 2490−2499

Thermotropic Ruthenium(II)-Containing Metallomesogens Based on Substituted 1,10-Phenanthroline Ligands

Thomas Cardinaels,* Jan Ramaekers, Kris Driesen, Peter Nockemann, Kristof Van Hecke, Luc Van Meervelt, Bart Goderis, and Koen Binnemans

Department of Chemistry, Katholieke Universiteit Leuven, Celestijnenlaan 200F - bus 2404, B-3001 Leuven, Belgium

Received September 16, 2008

Imidazo[4,5-f]-1,10-phenanthroline and pyrazino[2,3-f]-1,10-phenanthroline substituted with long alkyl chains are versatile ligands for the design of metallomesogens because of the ease of ligand substitution. Whereas the ligands and the corresponding rhenium(I) complexes were not liquid-crystalline, mesomorphism was observed for the corresponding ionic ruthenium(II) complexes with chloride, hexafluorophosphate, and bistriflimide counterions. The mesophases were identified as smectic A phases by high-temperature small-angle X-ray scattering (SAXS) using synchrotron radiation. The transition temperatures depend on the anion, the highest temperatures being observed for the chloride salts and the lowest for the bistriflimide salts. The ruthenium(II) complexes are examples of luminescent ionic liquid crystals.

Introduction

A versatile class of molecular materials, the class of *metallomesogens*, is obtained by incorporation of metals into liquid crystals.[1−3] The metal center adds additional functionality to the typical anisotropic properties of liquid crystals.[4] For instance, one can produce magnetic liquid crystals,[5−7] luminescent liquid crystals,[8−10] or redox-active liquid crystals.[11,12] The design of new metallomesogens is a challenge because the bulky metal fragments can disturb the subtle intramolecular forces that are responsible for the formation of mesophases.[13−15] The earliest examples of metallomesogens contained a metal center with a linear or square-planar coordination geometry so that these coordination compounds mimicked the rodlike or disklike shape of the conventional liquid crystals.[16,17] Nevertheless, most coordination compounds are limited to tetrahedral or octahedral centers. Moreover, magnetic or luminescent liquid crystals often make use of the unique properties of trivalent lanthanide ions,[2,18,19] and in general, these lanthanide(III) complexes have a coordination number of eight or nine.

* To whom correspondence should be addressed. E-mail: thomas.cardinaels@chem.kuleuven.be.

(1) *Metallomesogens, Synthesis, Properties and Applications*; Serrano, J. L., Ed.; VCH: Weinheim, Germany, 1996.
(2) Binnemans, K.; Görller-Walrand, C. *Chem. Rev.* **2002**, *102*, 2303–2345.
(3) Donnio, B.; Guillon, D.; Deschenaux, R.; Bruce, D. W. Metallomesogens. In *Comprehensive Coordination Chemistry II*; McCleverty, J. A.; Meyer, T. J., Eds.; Elsevier: Oxford, United Kingdom, 2003; pp 357−627.
(4) Bruce, D. W. *J. Chem. Soc., Dalton Trans.* **1993**, 2983–2989.
(5) Binnemans, K.; Galyametdinov, Y. G.; Van Deun, R.; Bruce, D. W.; Collinson, S. R.; Polishchuk, A. P.; Bikchantaev, I.; Haase, W.; Prosvirin, A. V.; Tinchurina, L.; Litvinov, I.; Gubajdullin, A.; Rakhmatullin, A.; Uytterhoeven, K.; Van Meervelt, L. *J. Am. Chem. Soc.* **2000**, *122*, 4335–4344.
(6) Galyametdinov, Y. G.; Athanassopoulou, M. A.; Griesar, K.; Kharitonova, O.; Bustamante, E. A. S.; Tinchurina, L.; Ovchinnikov, I. V.; Haase, W. *Chem. Mater.* **1996**, *8*, 922–926.
(7) Galyametdinov, Y. G.; Haase, W.; Goderis, B.; Moors, D.; Driesen, K.; Van Deun, R.; Binnemans, K. *J. Phys. Chem. B* **2007**, *111*, 13881–13885.
(8) Cavero, E.; Uriel, S.; Romero, P.; Serrano, J. L.; Gimenez, R. *J. Am. Chem. Soc.* **2007**, *129*, 11608–11618.
(9) Escande, A.; Guenee, L.; Nozary, H.; Bernardinelli, G.; Gumy, F.; Aebischer, A.; Bünzli, J. C. G.; Donnio, B.; Guillon, D.; Piguet, C. *Chem.—Eur. J.* **2007**, *13*, 8696–8713.
(10) Galyametdinov, Y. G.; Knyazev, A. A.; Dzhabarov, V. I.; Cardinaels, T.; Driesen, K.; Görller-Walrand, C.; Binnemans, K. *Adv. Mater.* **2008**, *20*, 252–257.
(11) Chang, H. C.; Shiozaki, T.; Kamata, A.; Kishida, K.; Ohmori, T.; Kiriya, D.; Yamauchi, T.; Furukawa, H.; Kitagawa, S. *J. Mater. Chem.* **2007**, *17*, 4136–4138.
(12) Turpin, F.; Guillon, D.; Deschenaux, R. *Mol. Cryst. Liq. Cryst.* **2001**, *362*, 171–175.
(13) Binnemans, K.; Lodewyckx, K. *Angew. Chem., Int. Ed.* **2001**, *40*, 242–244.
(14) Bruce, D. W. *Adv. Mater.* **1994**, *6*, 699–701.
(15) Date, R. W.; Iglesias, E. F.; Rowe, K. E.; Elliott, J. M.; Bruce, D. W. *Dalton Trans.* **2003**, 1914–1931.
(16) Giroud-Godquin, A. M.; Maitlis, P. M. *Angew. Chem., Int. Ed.* **1991**, *30*, 375–402.
(17) Hudson, S. A.; Maitlis, P. M. *Chem. Rev.* **1993**, *93*, 861–885.
(18) Piguet, C.; Bünzli, J. C. G.; Donnio, B.; Guillon, D. *Chem. Commun.* **2006**, 3755–3768.

10.1021/ic801772q CCC: $40.75
Published on Web 02/11/2009

Different approaches toward high coordination number metallomesogens have been developed. The most popular approach is to attach many alkyl chains to the parent coordination compound, and this method usually leads to the formation of columnar mesophases.[20,21] Another popular approach is to connect the metal-containing building block via long, flexible alkyl spacers to mesophase-inducing groups like the cholesteryl group or the cyanobiphenyl group.[22,23] Here the liquid-crystalline properties mainly depend on the number and type of mesogenic groups and not on the metal-containing unit. A third approach, which has so far largely been neglected, is by taking advantage of electrostatic interactions. Research on ionic liquid crystals is becoming more and more popular, but most of these studies are not focused on the design of high coordination number metallomesogens.[24−27] A very nice example of the power of having electrostatic interactions for the stabilization of mesophases is found in the seminal work of Piechocki et al. on liquid-crystalline bis(phthalocyaninato)lanthanide(III) complexes.[28] This is the first paper about discotic lanthanidomesogens, and the authors illustrate that it is possible to oxidize to neutral phthalocyanine sandwich compound. The transition temperatures of the oxidized complexes are quite different to those of the neutral compound, and oxidation has a stabilizing effect on the mesophase. For instance the lutetium(III) compound with eight peripheral dodecyloxymethyl chains, $[(C_{12}H_{25}OCH_2)_8Pc]_2Lu$, forms a hexagonal columnar phase between 24 and 30 °C, whereas the oxidized analogue $[(C_{12}H_{25}OCH_2)_8Pc]_2Lu^+SbCl_6^-$ forms the same phase between 13 and 118 °C. Even more striking is the example of the octyloxymethyl derivative: $[(C_8H_{17}OCH_2)_8Pc]_2Lu$ is not liquid-crystalline and melts at 25 °C, whereas $[(C_8H_{17}OCH_2)_8Pc]_2Lu^+SbCl_6^-$ forms a hexagonal columnar phase between 10 and 130 °C. A similar mesophase stabilizing effect upon oxidation was observed for the bis(phthalocyaninato)lanthanide(III) complexes with alkoxy chains.[29] Another example of inducing mesomorphism via electrostatic interactions is the chemical oxidation of a non-mesomorphic ferrocene derivative into the corresponding ferrocenium species, which exhibits a smectic A phase.[30]

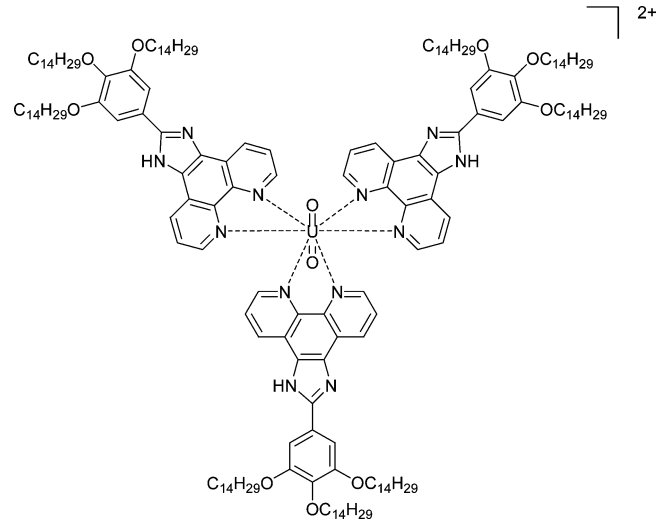

Figure 1. Structure of the uranyl complex. The two noncoordinating triflate counterions have been omitted.

Recently, we introduced imidazo[4,5-f]-1,10-phenanthrolines as a new class of ligands for the design of metallomesogens.[23,31] These imidazo[4,5-f]-1,10-phenanthrolines are versatile ligands because of their easy substitution and because they can coordinate to various metal ions, leading to complexes with different ligand-to-metal ratios. By attaching cyanobiphenyl groups via long alkyl spacers to the parent ligand, it was possible to design the first examples of nematogenic lanthanide(III) complexes. However, the results for the imidazo[4,5-f]-1,10-phenanthrolines with alkyl chains (without mesogenic groups attached) were rather disappointing because none of the ligands and only few metal complexes showed liquid-crystalline behavior.[31] One of the most interesting metal complexes was the uranyl compound with three imidazo[4,5-f]-1,10-phenanthroline ligands and triflate counterions, which exhibited a hexagonal columnar phase over a wide temperature range (Figure 1).[32] In this case, the electrostatic interactions between the anions and the large cationic cores appear to play a substantial role in promoting the liquid crystal phase, although the propeller-like shape of the uranyl complex is nicely set up for columnar mesomorphism. In this paper, we present another example of promotion of liquid-crystalline behavior by electrostatic interactions. The neutral rhenium(I) complexes of the imidazo[4,5-f]-1,10-phenanthrolines and the similar pyrazino[2,3-f]-1,10-phenanthrolines are not liquid-crystalline, whereas the corresponding ionic ruthenium(II) complexes form a smectic A mesophase. However, the hypothesis that electrostatic interactions would be the only driving force for the formation of these liquid crystal phases is too strict. We are convinced

(19) Terazzi, E.; Suarez, S.; Torelli, S.; Nozary, H.; Imbert, D.; Mamula, O.; Rivera, J. P.; Guillet, E.; Benech, J. M.; Bernardinelli, G.; Scopelliti, R.; Donnio, B.; Guillon, D.; Bünzli, J. C. G.; Piguet, C. *Adv. Funct. Mater.* **2006**, *16*, 157–168.
(20) Binnemans, K.; Lodewyckx, K.; Donnio, B.; Guillon, D. *Chem.—Eur. J.* **2002**, *8*, 1101–1105.
(21) Trzaska, S. T.; Zheng, H. X.; Swager, T. M. *Chem. Mater.* **1999**, *11*, 130–134.
(22) Campidelli, S.; Vazquez, E.; Milic, D.; Prato, M.; Barbera, J.; Guldi, D. M.; Marcaccio, M.; Paolucci, D.; Paolucci, F.; Deschenaux, R. *J. Mater. Chem.* **2004**, *14*, 1266–1272.
(23) Cardinaels, T.; Driesen, K.; Parac-Vogt, T. N.; Heinrich, B.; Bourgogne, C.; Guillon, D.; Donnio, B.; Binnemans, K. *Chem. Mater.* **2005**, *17*, 6589–6598.
(24) Binnemans, K. *Chem. Rev.* **2005**, *105*, 4148–4204.
(25) Kato, T.; Mizoshita, N.; Kishimoto, K. *Angew. Chem., Int. Ed.* **2006**, *45*, 38–68.
(26) Bruce, D. W. *Acc. Chem. Res.* **2000**, *33*, 831–840.
(27) Vacatello, M.; Degirolamo, M.; Busico, V. *J. Chem. Soc., Faraday Trans. I* **1981**, *77*, 2367–2375.
(28) Piechocki, C.; Simon, J.; Andre, J. J.; Guillon, D.; Petit, P.; Skoulios, A.; Weber, P. *Chem. Phys. Lett.* **1985**, *122*, 124–128.
(29) Belarbi, Z.; Sirlin, C.; Simon, J.; Andre, J. J. *J. Phys. Chem.* **1989**, *93*, 8105–8110.
(30) Deschenaux, R.; Schweissguth, M.; Levelut, A. M. *Chem. Commun.* **1996**, 1275–1276.
(31) Cardinaels, T.; Ramaekers, J.; Nockemann, P.; Driesen, K.; Van Hecke, K.; Van Meervelt, L.; Lei, S. B.; De Feyter, S.; Guillon, D.; Donnio, B.; Binnemans, K. *Chem. Mater.* **2008**, *20*, 1278–1291.
(32) Cardinaels, T.; Ramaekers, J.; Guillon, D.; Donnio, B.; Binnemans, K. *J. Am. Chem. Soc.* **2005**, *127*, 17602–17603.

that the electrostatic interactions are of prime importance, but is it necessary to mention that also other interactions play a role. For instance, considering the head groups of the ligands, the rhenium(I) complexes, and the ruthenium(II) complexes, there is a large difference in size, shape, and steric hindrence. In addition, in the case of the ruthenium(II) complexes, π-π interactions may exist between the head groups. A structural model of the mesophase is proposed on the basis of small-angle X-ray scattering using synchrotron radiation. The transition temperatures of the ionic metallomesogens could be tuned by changing the counterion. Examples of ruthenium(II)-containing thermotropic metallomesogens are scarce.[33−37] Lytropic ruthenium(II) complexes have been studied because they can act as a template for supported heterogeneous ruthenium catalysts.[38−41] Ruthenium(II) complexes are also of interest because of their excellent photophysical properties,[42−45] so that ruthenium(II)-containing metallomesogens form a class of luminescent liquid crystals. In this paper, the luminescence properties of the new ionic liquid-crystalline ruthenium(II) complexes are described.

Experimental Section

General Procedures. Nuclear magnetic resonance (NMR) spectra were recorded on a Bruker Avance 300 spectrometer (operating at 300 MHz for ^{1}H) or a Bruker AMX-400 spectrometer (operating at 400 MHz for ^{1}H). Elemental analyses were obtained on a CE Instruments EA-1110 elemental analyzer. Optical textures of the mesophases were observed with an Olympus BX60 polarizing microscope equipped with a LINKAM THMS600 hot stage and a LINKAM TMS93 programmable temperature controller. DSC traces were recorded with a Mettler-Toledo DSC822e module. Electrospray ionization (ESI) spectra were recorded on a Thermo Finnigan LCQ Advantage mass spectrometer.

Small-angle X-ray experiments were carried out at the Dutch−Belgian Beamline (DUBBLE, BM26-B) of the European Synchrotron Radiation Facility (ESRF, Grenoble).[46] Data were collected using a X-ray wavelength, λ, of 0.775 Å nm on a two-dimensional position sensitive gas-filled wire chamber detector at 1.5 m from the sample. The covered scattering vector range $0.045 < q < 0.8$ Å^{-1} was calibrated with a silver behenate specimen ($q = (4\pi/\lambda) \sin\theta$, where 2θ is the scattering angle).[47] The isotropic data were corrected for the detector response, azimuthally integrated, and normalized to the intensity of the primary beam, measured by an ionization chamber placed downstream from the sample. The background scattering due to the experimental setup and the sample holder was subtracted according to standard procedures, taking into account transmission differences. The samples, sealed in aluminum pans, were mounted into a Linkam HFS 191 hot-stage for temperature control.

Red-brown single crystals of $[Ru(bipy)_2(dppz(Cl_2))]Cl_2 \cdot (H_2O)_4 \cdot (C_2H_5OH)$ were obtained by slow evaporation of a solution of the compound in ethanol at room temperature. X-ray intensity data were collected on a SMART 6000 diffractometer equipped with CCD detector using Cu Kα radiation ($\lambda = 1.54178$ Å). The images were interpreted and integrated with the program SAINT from Bruker.[48] Crystallographic data for $[Ru(bipy)_2(dppz(Cl_2))]Cl_2 \cdot (H_2O)_4 \cdot (C_2H_5OH)$: $C_{40}H_{38}Cl_4N_8O_5Ru$, $M = 953.65$ g mol^{-1}, monoclinic, $P2_1/c$ (No. 2), $a = 10.4063(6)$ Å, $b = 17.9289(11)$ Å, $c = 21.8226(11)$ Å, $\beta = 99.386(3)°$, $V = 4017.0(4)$ Å^3, $T = 100(2)$ K, $Z = 4$, $\rho_{calc} = 1.577$ g cm^{-3}, μ(Cu Kα) = 6.073 mm^{-1}, $F(000) = 1944$, crystal size 0.14 × 0.14 × 0.1 mm, 37739 measured reflections, 7713 independent reflections, $R_{int} = 0.0972$. Final $R = 0.0374$ for 5778 reflections with $I > 2\sigma(I)$ and $\omega R2 = 0.0915$ for all data.

The structure was solved by direct methods and refined by full-matrix least-squares on F^2 using the SHELXTL program package.[49] Non-hydrogen atoms were anisotropically refined, and the hydrogen atoms in the riding mode with isotropic temperature factors fixed at 1.2 times U(eq) of the parent atoms (1.5 times for methyl groups). CCDC-690425 contains the supplementary crystallographic data for this paper. These data can be obtained free of charge via www.cam.ac.uk/conts/retrieving.html (or from the Cambridge Crystallographic Data Centre, 12 Union Road, Cambridge CB2 1EZ, UK; fax: (+44−1223−336033; or deposit@ccdc.cam.uk). The hydrogen atoms of the four water molecules and the OH-function of the ethanol molecule were found in the Fourier difference map and refined with a restrained O−H distance of 0.84 Å.

Synthetic Procedures. The molecular structure of $\mathbf{L_I}$, $\mathbf{L_{II}}$, and $\mathbf{P_I}$ is shown in Scheme 1.

Synthesis of $\mathbf{L_I}$ (1). $\mathbf{L_I}$ was synthesized following a literature procedure:[31] 3,4-Dioctadecyloxybenzaldehyde (0.0020 mol, 1.29 g) was added to a warm solution of 1,10-phenanthroline-5,6-dione (0.0020 mol, 0.42 g) and ammonium acetate (0.0170 mol, 1.32 g) in 20 mL of glacial acetic acid. The mixture was heated to 85 °C for 5 h. After the reaction mixture was cooled to room temperature, it was poured into 100 mL of water and neutralized to pH 7 with an aqueous ammonia solution. The orange precipitate was filtered off, washed with distilled water and dried. The crude product was purified on a silica column with $CHCl_3$/hexane/MeOH (50:50:10) as the eluent. Since the compound holds solvents firmly, it was

(33) Barral, M. C.; Jimenez-Aparicio, R.; Priego, J. L.; Royer, E. C.; Torres, M. R.; Urbanos, F. A. *Inorg. Chem. Commun.* **1999**, *2*, 153–155.
(34) Bonnet, L.; Cukiernik, F. D.; Maldivi, P.; Giroudgodquin, A. M.; Marchon, J. C.; Ibnelhaj, M.; Guillon, D.; Skoulios, A. *Chem. Mater.* **1994**, *6*, 31–38.
(35) Caplan, J. F.; Murphy, C. A.; Swansburg, S.; Lemieux, R. P.; Cameron, T. S.; Aquino, M. A. S. *Can. J. Chem.* **1998**, *76*, 1520–1523.
(36) Deschenaux, R.; Donnio, B.; Rheinwald, G.; Stauffer, F.; Süss-Fink, G.; Velker, J. *J. Chem. Soc., Dalton Trans.* **1997**, 4351–4355.
(37) Frein, S.; Auzias, M.; Sondenecker, A.; Vieille-Petit, L.; Guintchin, B.; Maringa, N.; Süss-Fink, G.; Barbera, J.; Deschenaux, R. *Chem. Mater.* **2008**, *20*, 1340–1343.
(38) Bruce, D. W.; Holbrey, J. D.; Tajbakhsh, A. R.; Tiddy, G. J. T. *J. Mater. Chem.* **1993**, *3*, 905–906.
(39) Danks, M. J.; Jervis, H. B.; Nowotny, M.; Zhou, W. Z.; Maschmeyer, T. A.; Bruce, D. W. *Catal. Lett.* **2002**, *82*, 95–98.
(40) Holbrey, J. D.; Tiddy, G. J. T.; Bruce, D. W. *J. Chem. Soc., Dalton Trans.* **1995**, 1769–1774.
(41) Jervis, H. B.; Raimondi, M. E.; Raja, R.; Maschmeyer, T.; Seddon, J. M.; Bruce, D. W. *Chem. Commun.* **1999**, 2031–2032.
(42) Balzani, V.; Barigelletti, F.; Decola, L. *Top. Curr. Chem.* **1990**, *158*, 31–71.
(43) Balzani, V.; Ceroni, P.; Juris, A.; Venturi, M.; Campagna, S.; Puntoriero, F.; Serroni, S. *Coord. Chem. Rev.* **2001**, *219*, 545–572.
(44) Nakamaru, K. *Bull. Chem. Soc. Jpn.* **1982**, *55*, 2697–2705.
(45) Sauvage, J. P.; Collin, J. P.; Chambron, J. C.; Guillerez, S.; Coudret, C.; Balzani, V.; Barigelletti, F.; Decola, L.; Flamigni, L. *Chem. Rev.* **1994**, *94*, 993–1019.
(46) Bras, W.; Dolbnya, I. P.; Detollenaere, D.; van Tol, R.; Malfois, M.; Greaves, G. N.; Ryan, A. J.; Heeley, E. *J. Appl. Crystallogr.* **2003**, *36*, 791–794.
(47) Huang, T. C.; Toraya, H.; Blanton, T. N.; Wu, Y. *J. Appl. Crystallogr.* **1993**, *26*, 180–184.
(48) *SAINT*, version 5/6.0; Bruker Analytical X-ray Systems Inc.: Madison, WI, 1997.
(49) *SHELXTL-PC*, version 5.1; Bruker Analytical X-ray Systems Inc.: Madison, WI, 1997.

Scheme 1. (i) CH_3COOH, CH_3COONH_4, 85 °C; (ii) CH_3COOH, 100 °C; (iii) $C_{18}H_{37}SH$, K_2CO_3, DMF, 85 °C

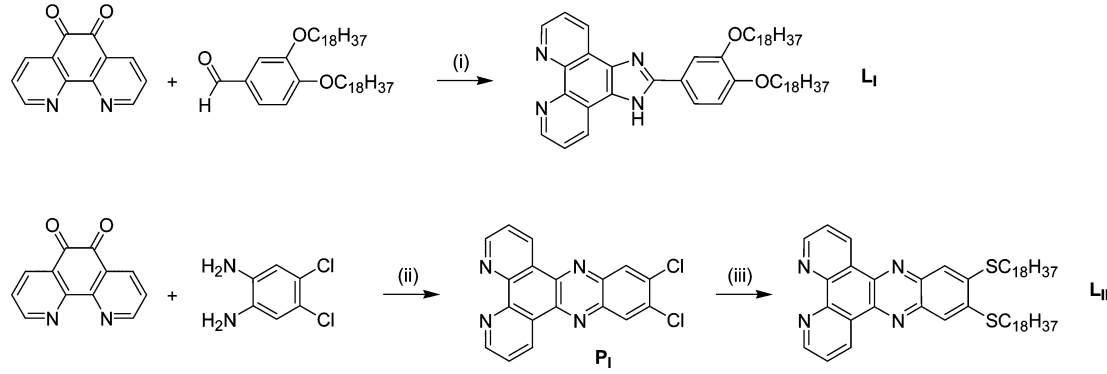

dried in a vacuum oven at 50 °C. Yield: 30% (0.50 g). δ_H (400 MHz, THF-d_8): 0.87 (t, 6H, CH_3, $J = 6.4$ Hz), 1.28−1.76 (m, 64H, CH_2), 3.52 (t, 2H, CH_2−O, $J = 6.2$ Hz), 3.96 (t, 2H, CH_2−O, $J = 6.3$ Hz), 6.93 (d, 1H, H-aryl, $J_o = 8.4$ Hz), 7.30 (b, m, 1H, H-aryl), 7.72 (b, m, 1H, H-aryl), 7.92−7.96 (m, 2H, H-aryl), 8.73 (b, m, 2H, H-aryl), 8.95 (b, d, 1H, H-aryl), 9.13 (b, d, 1H, H-aryl), 14.40 (b, s, 1H, N−H). Calcd. for $C_{55}H_{84}N_4O_2 \cdot 0.5H_2O$ (833.28): C 78.43, H 10.17, N 6.65. Found: C 78.47, H 9.77, N 6.78. ESI-MS (methanol, *m/z*): 833.9, $[M + H]^+$. M.p.: 116 °C.

Synthesis of P_I (2). 1,10-Phenanthroline-5,6-dione (0.0024 mol, 0.50 g) and 4,5-dichlorobenzene-1,2-diamine (0.0048 mol, 0.85 g) were heated under reflux in glacial acetic acid for 2 h. The resulting green precipitate was filtered off, washed with water, ethanol, acetone, and diethyl ether, and dried in a vacuum oven at 50 °C. Yield: 80% (0.67 g). δ_H (300 MHz, $CDCl_3$): 7.76 (dd, 2H, H-aryl, $J_o = 7.8$ Hz, $J_o = 4.1$ Hz), 8.38 (s, 2H, H-aryl), 9.26 (dd, 2H, H-aryl, $J_o = 4.1$ Hz, $J_m = 1.6$ Hz), 9.43 (dd, 2H, H-aryl, $J_o = 7.8$ Hz, $J_m = 1.6$ Hz). Calcd. for $C_{18}H_8Cl_2N_4$ (351.19): C 61.56, H 2.30, N 15.95. Found: C 61.49, H 2.65, N 15.68. ESI-MS (methanol, *m/z*): 351.4, $[M + H]^+$. M.p.: 355 °C.

Synthesis of L_{II} (3). Octadecanethiol (0.0056 mol, 1.60 g) and potassium carbonate (0.0018 mol, 2.53 g) were added to a solution of P_I (0.0014 mol, 0.49 g) in 100 mL of DMF. The mixture was heated to 85 °C and stirred for 5 days. Then, the reaction mixture was poured into water, and the resulting yellow precipitate was filtered off, washed with water, and dried. The crude product was purified on a silica column with CH_2Cl_2/MeOH (95:5) as the eluent. Yield: 60% (0.72 g). δ_H (300 MHz, $CDCl_3$): 0.87 (b, t, 6H, CH_3), 1.25−1.39 (m, 56H, CH_2), 1.55−1.59 (m, 4H, CH_2), 1.86−1.96 (m, 4H, C**H**$_2$-CH_2−S), 3.25 (t, 4H, CH_2−S, $J = 7.6$ Hz), 7.77−7.82 (m, 2H, H-aryl), 8.02 (s, 2H, H-aryl), 9.27 (d, 2H, H-aryl, $J_o = 4.3$ Hz), 9.61 (d, 2H, H-aryl, $J_o = 8.3$ Hz). Calcd. for $C_{54}H_{82}N_4S_2 \cdot 0.5H_2O$ (851.39): C 75.38, H 9.72, N 6.51. Found: C 75.20, H 10.21, N 6.28. ESI-MS (methanol, *m/z*): 852.3, $[M + H]^+$. M.p.: 119 °C.

Synthesis of $[ReBr(CO)_3L_{II}]$ (4). Rhenium(I) pentacarbonyl bromide (0.00012 mol, 0.049 g) was added to a solution of L_{II} (0.00012 mol, 0.10 g) in toluene, and the mixture was refluxed for 3 h. Then the solvent was removed under reduced pressure, and the crude product was purified on a silica column with $CHCl_3$/hexane (50:50) as the eluent. The complex was dissolved in a minimum amount of $CHCl_3$ and precipitated in methanol. The yellow precipitate was filtered off and dried in a vacuum oven at 50 °C. Yield: 64% (0.092 g). δ_H (300 MHz, $CDCl_3$): δ_H (300 MHz, $CDCl_3$): 0.88 (t, 6H, CH_3, $J = 6.4$ Hz), 1.26−1.44 (m, 52H, CH_2), 1.52−1.66 (m, 8H, CH_2), 1.88−1.98 (m, 4H, C**H**$_2$−CH_2−S), 3.27 (t, 4H, CH_2−S, $J = 7.2$ Hz), 7.95−7.99 (m, 4H, H-aryl), 9.44 (d, 2H, H-aryl, $J_o = 5.5$ Hz), 9.73 (d, 2H, H-aryl, $J_o = 8.2$ Hz). Calcd. for $C_{57}H_{82}BrN_4O_3ReS_2$ (1201.53): C 56.98, H 6.88, N 4.66. Found: C 57.06, H 7.20, N 4.40. ESI-MS (methanol, *m/z*): 1223.4, $[M + Na]^+$. M.p.: 205 °C.

Synthesis of *cis*-$[RuCl_2(bipy)_2]$ (5). *cis*-$[RuCl_2(bipy)_2]$ was synthesized following a literature procedure:[50] a mixture of $RuCl_3 \cdot 3H_2O$ (0.0070 mol, 1.83 g), 2,2′-bipyridine (0.0140 mol, 2.20 g), LiCl (0.0470 mol, 2.00 g), and 20 mL of DMF was refluxed for 8 h. Then the mixture was cooled, and 150 mL of acetone was added. The precipitate was filtered off and washed 3 times with 25 mL of water and 3 times with 25 mL of diethyl ether. The dark green microcrystalline product was dried under vacuum. Yield: 47% (1.61 g). Calcd. for $C_{20}H_{16}Cl_2N_4Ru \cdot 0.5H_2O$ (484.34): C 48.69, H 3.47, N 11.36. Found: C 48.88, H 3.65, N 11.49. ESI-MS (methanol, *m/z*): 485.1, $[M + H]^+$.

Synthesis of $[Ru(bipy)_2L_I](PF_6)_2$ (6). *cis*-$[RuCl_2(bipy)_2]$ (0.0015 mol, 0.73 g) was dissolved in 100 mL of a warm ethanol/water (7:3, v/v) mixture under a nitrogen atmosphere, and the solution was stirred for 1 h at 80 °C. Then L_I (0.0015 mol, 1.22) was added, and the mixture was refluxed overnight under a nitrogen atmosphere after which the solution became clearly red. Ethanol was removed under reduced pressure, and a saturated solution of KPF_6 in water was added. A red precipitate was formed, filtered off, and washed with water. The crude product was purified on an alumina column with acetonitrile/toluene (2:1, v/v) as the eluent. The product was dissolved in a minimum amount of ethanol and precipitated in hexane. The orange-red precipitate was filtered off and dried in a vacuum oven at 50 °C. Yield: 79% (1.76 g). δ_H (300 MHz, $CDCl_3$): 0.85−0.89 (m, 6H, CH_3), 1.24−1.25 (m, 56H, CH_2), 1.42−1.49 (m, 4H, CH_2), 1.81 (b, m, 4H, C**H**$_2$-CH_2−O), 3.99 (b, t, 2H, CH_2−O), 4.10 (b, t, 2H, CH_2−O), 6.94 (d, 1H, H-aryl, $J_o = 6.1$ Hz), 7.16−7.24 (m, 2H, H-aryl), 7.37−7.46 (m, 3H, H-aryl), 7.53−7.60 (m, 2H, H-aryl), 7.73−7.77 (m, 3H, H-aryl), 7.84−7.97 (m, 8H, H-aryl), 8.37−8.43 (m, 4H, H-aryl), 9.04−9.09 (m, 2H, H-aryl), 11.95 (b, s, 1H, N−H). Calcd. for $C_{75}H_{100}F_{12}N_8O_2P_2Ru$ (1536.65): C 58.62, H 6.56, N 7.29. Found: C 58.47, H 6.82, N 7.01. ESI-MS (methanol, *m/z*): 623.7, $[M - 2PF_6]^{2+}$.

Synthesis of $[Ru(bipy)_2L_{II}](PF_6)_2$ (7). $[Ru(bipy)_2L_{II}](PF_6)_2$ was prepared starting from *cis*-$[RuCl_2(bipy)_2]$ (0.0006 mol, 0.30 g) and L_{II} (0.0006 mmol, 0.53 g) using the same procedure as described for $[Ru(bipy)_2L_I](PF_6)_2$ to yield the product as a red powder. Yield: 74% (1.30 g). δ_H (400 MHz, $CDCl_3$): 0.87 (t, 6H, CH_3, $J = 6.8$ Hz), 1.25−1.42 (m, 56H, CH_2), 1.55−1.62 (m, 4H, CH_2), 1.86−1.93 (m, 4H, C**H**$_2$-CH_2−S), 3.24 (t, 4H, CH_2−S, $J = 7.2$ Hz), 7.35 (t, 2H, H-aryl, $J = 6.5$ Hz), 7.52 (t, 2H, H-aryl, $J = 6.4$ Hz), 7.74 (d, 2H, H-aryl, $J_o = 5.3$ Hz), 7.87 (d, 2H, H-aryl, $J_o = 5.2$ Hz), 7.90−7.95 (m, 4H, H-aryl), 7.97 (s, 2H, H-aryl), 8.02 (t, 2H, H-aryl,

(50) Sullivan, B. P.; Salmon, D. J.; Meyer, T. J. *Inorg. Chem.* **1978**, *17*, 3334–3341.

J = 7.76 Hz), 8.17 (d, 2H, H-aryl, J_o = 4.88 Hz), 8.41−8.46 (m, 4H, H-aryl), 9.60 (d, 2H, H-aryl, J_o = 8.1 Hz). Calcd. for $C_{74}H_{98}F_{12}N_8P_2RuS_2$ (1554.75): C 57.17, H 6.35, N 7.21. Found: C 56.98, H 6.50, N 6.95. ESI-MS (methanol, *m/z*): 1409.6, $[M - PF_6]^+$.

Synthesis of $[Ru(bipy)_2L_I]Cl_2$ (8). A saturated solution of LiCl in acetone was added to a solution of $[Ru(bipy)_2\mathbf{L_I}](PF_6)_2$ (0.0008 mol, 1.21 g) in 20 mL of acetone. An orange-red precipitate was formed, filtered off, washed with acetone, and dried in a vacuum oven at 50 °C. Yield: 98% (1.01 g). δ_H (300 MHz, $CDCl_3$): 0.87 (t, 6H, CH_3, J = 6.3 Hz), 1.25−1.56 (m, 60H, CH_2), 1.79−1.92 (m, 4H, C**H**$_2$-CH_2−O), 4.05 (t, 2H, CH_2−O, J = 6.5 Hz), 4.28 (t, 2H, CH_2−O, J = 6.4 Hz), 7.00 (d, 1H, H-aryl, J_o = 8.5 Hz), 7.23−7.34 (m, 2H, H-aryl), 7.46−7.47 (m, 1H, H-aryl), 7.52−7.65 (m, 4H, H-aryl), 7.74−7.89 (m, 5H, H-aryl), 8.01−8.06 (m, 2H, H-aryl), 8.10−8.19 (m, 2H, H-aryl), 8.24−8.25 (m, 1H, H-aryl), 8.33 (d, 1H, H-aryl, J_o = 7.9 Hz), 8.86−8.92 (m, 2H, H-aryl), 9.04 (d, 1H, H-aryl, J_o = 7.9 Hz), 9.10 (d, 1H, H-aryl, J_o = 7.8 Hz), 9.18 (d, 1H, H-aryl, J_o = 8.1 Hz), 10.38 (d, 1H, H-aryl, J_o = 8.0 Hz), 15.43 (b, s, 1H, N−H). Calcd. for $C_{75}H_{100}Cl_2N_8O_2Ru$ (1317,62): C 68.37, H 7.65, N 8.50. Found: C 68.12, H 7.73, N 8.35. ESI-MS (methanol, *m/z*): 623.4, $[M - 2Cl]^{2+}$.

Synthesis of $[Ru(bipy)_2L_{II}]Cl_2$ (9). $[Ru(bipy)_2\mathbf{L_{II}}]Cl_2$ was prepared starting from $[Ru(bipy)_2\mathbf{L_{II}}](PF_6)_2$ (0.0003 mol, 0.40 g) using the same procedure as described for $[Ru(bipy)_2\mathbf{L_I}]Cl_2$ to yield the product as a red powder. Yield: 91% (0.31 g). δ_H (400 MHz, $CDCl_3$): 0.87 (t, 6H, CH_3, J = 6.8 Hz), 1.25−1.45 (m, 56H, CH_2), 1.56−1.63 (m, 4H, CH_2), 1.87−1.95 (m, 4H, C**H**$_2$−CH_2−S), 3.26 (t, 4H, CH_2−S, J = 6.8 Hz), 7.42 (t, 2H, H-aryl, J = 6,1 Hz), 7.63 (t, 2H, H-aryl, J = 5.9 Hz), 7.86 (d, 2H, H-aryl, J_o = 4.8 Hz), 7.97−8.11 (m, 8H, H-aryl), 8,16 (t, 2H, H-aryl, J = 7.44 Hz), 8.40 (d, 2H, H-aryl, J_o = 3.6 Hz), 8.91−8.96 (m, 4H, H-aryl), 9.65 (d, 2H, H-aryl, J_o = 7.9 Hz). Calcd. for $C_{74}H_{98}Cl_2N_8RuS_2$ (1335,73): C 66.54, H 7.40, N 8.39. Found: C 66.25, H 7.55, N 8.22. ESI-MS (methanol, *m/z*): 632.6, $[M - 2Cl]^{2+}$.

Synthesis of $[Ru(bipy)_2L_I](NTf_2)_2$ (10). A saturated solution of lithium bis(trifluoromethylsulfonyl)imide ($LiNTf_2$) in water was added to a solution of $[Ru(bipy)_2\mathbf{L_I}]Cl_2$ (0.0006 mol, 0.78 g) in 50 mL of a warm ethanol/water (1:5, v/v) mixture. An orange-red precipitate was formed, filtered off, washed with water and dried in a vacuum oven at 50 °C. Yield: 82% (0.87 g). δ_H (300 MHz, $CDCl_3$): 0.87 (t, 6H, CH_3, J = 6.3 Hz), 1.25−1.48 (m, 60H, CH_2), 1.79−1.89 (m, 4H, C**H**$_2$−CH_2−O), 4.04 (t, 2H, CH_2−O, J = 6.4 Hz), 4.12 (t, 2H, CH_2−O, J = 6.2 Hz), 6.99 (d, 1H, H-aryl, J_o = 8.4 Hz), 7.22−7.28 (m, 2H, H-aryl), 7.44−7.55 (m, 4H, H-aryl), 7.72−8.07 (m, 12H, H-aryl), 8.44−8.50 (m, 4H, H-aryl), 9.15 (d, 2H, H-aryl, J_o = 8.2 Hz), 12.13 (b, s, 1H, N−H). Calcd. for $C_{79}H_{100}F_{12}N_{10}O_{10}RuS_4$ (1807.01): C 52.51, H 5.58, N 7.75. Found: C 52.41, H 5.15, N 7.49. ESI-MS (methanol, *m/z*): 1526.3, $[M - NTf_2]^+$.

Synthesis of $[Ru(bipy)_2L_{II}](NTf_2)_2$ (11). $[Ru(bipy)_2\mathbf{L_{II}}](NTf_2)_2$ was prepared starting from $[Ru(bipy)_2\mathbf{L_{II}}]Cl_2$ (0.0001 mmol, 0.15 g) using the same procedure as described for $[Ru(bipy)_2\mathbf{L_I}](NTf_2)_2$ to yield the product as a red powder. Yield: 90% (0.18 g). δ_H (300 MHz, $CDCl_3$): 0.87 (t, 6H, CH_3, J = 6.5 Hz), 1.25−1.45 (m, 56H, CH_2), 1.52−1.62 (m, 4H, CH_2), 1.87−1.94 (m, 4H, C**H**$_2$−CH_2−S), 3.27 (t, 4H, CH_2−S, J = 7.3 Hz), 7.36−7.40 (m, 2H, H-aryl), 7.57−7.61 (m, 2H, H-aryl), 7.79 (d, 2H, H-aryl, J_o = 5.3 Hz), 7.93−8.12 (m, 10H, H-aryl), 8.24 (d, 2H, H-aryl, J_o = 4.8 Hz), 8.39−8.45 (m, 4H, H-aryl), 9.67 (d, 2H, H-aryl, J_o = 8.1 Hz). Calcd. for $C_{78}H_{98}F_{12}N_{10}O_8RuS_6$ (1825.12): C 51.33, H 5.41, N 7.67. Found: C 50.86, H 5.53, N 7.20. ESI-MS (methanol, *m/z*): 1544.6, $[M - NTf_2]^+$.

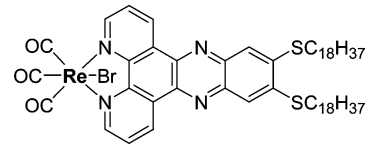

Figure 2. Molecular structure of $[ReBr(CO)_3\mathbf{L_{II}}]$.

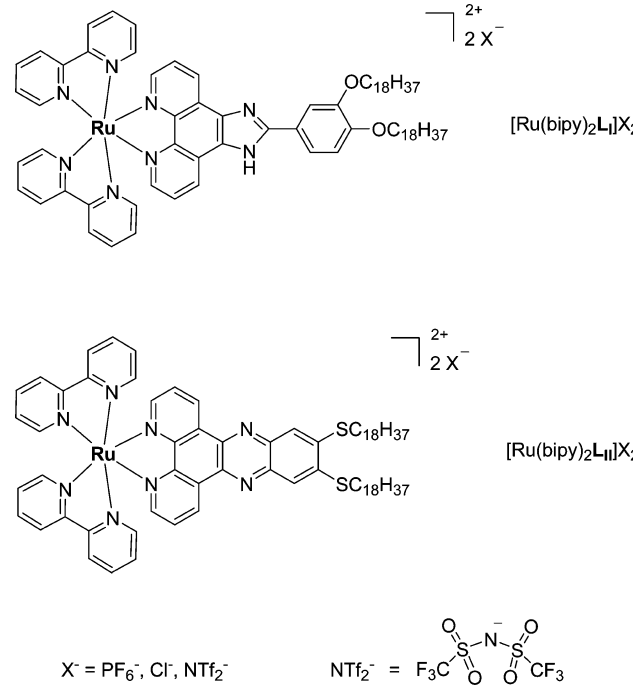

Figure 3. Molecular structure of the ruthenium(II) complexes.

Results and Discussion

Synthesis. The synthesis of the ligands $\mathbf{L_I}$ and $\mathbf{L_{II}}$ is outlined in Scheme 1. The 2-substituted imidazo[4,5-f]-1,10-phenanthroline$\mathbf{L_I}$ was prepared by a condensation reaction between 1,10-phenanthroline-5,6-dione and 3,4-dioctadecyloxybenzaldehyde, following a literature procedure.[31] The pyrazino[2,3-f]-1,10-phenanthroline$\mathbf{L_{II}}$ was synthesized via two reaction steps. The first step consists of the condensation between 1,10-phenanthroline-5,6-dione and 4,5-dichlorobenzene-1,2-diamine to afford precursor $\mathbf{P_I}$. The second step is the nucleophilic aromatic substitution of $\mathbf{P_I}$ by 1-octadecanethiolate.[51]

The rhenium(I) complex $[ReBr(CO)_3\mathbf{L_{II}}]$ was prepared by reaction between $\mathbf{L_{II}}$ and $[ReBr(CO)_5]$ (1:1 molar ratio) in toluene. The molecular structure of $[ReBr(CO)_3\mathbf{L_{II}}]$ is presented in Figure 2.

The molecular structure of the ruthenium(II) complexes is shown in Figure 3. Crude $[Ru(bipy)_2\mathbf{L_I}]Cl_2$ and $[Ru(bipy)_2\mathbf{L_{II}}]Cl_2$ were prepared by a reaction between $\mathbf{L_I}$ and $\mathbf{L_{II}}$, respectively, and *cis*-$[RuCl_2(bipy)_2]$. Then, crude $[Ru(bipy)_2\mathbf{L_I}](PF_6)_2$ and $[Ru(bipy)_2\mathbf{L_{II}}](PF_6)_2$ were synthesized by a metathesis reaction between crude $[Ru(bipy)_2\mathbf{L_I}]Cl_2$ and $[Ru(bipy)_2\mathbf{L_{II}}]Cl_2$, respectively, and potassium hexafluorophosphate. $[Ru(bipy)_2\mathbf{L_I}](PF_6)_2$ and $[Ru(bipy)_2\mathbf{L_{II}}](PF_6)_2$ were purified by column chromatography on alumina. This synthetic sequence was used because it is not possible to

(51) Kestemont, G.; de Halleux, V.; Lehmann, M.; Ivanov, D. A.; Watson, M. D.; Geerts, Y. H. *Chem. Commun.* **2001**, 2074–2075.

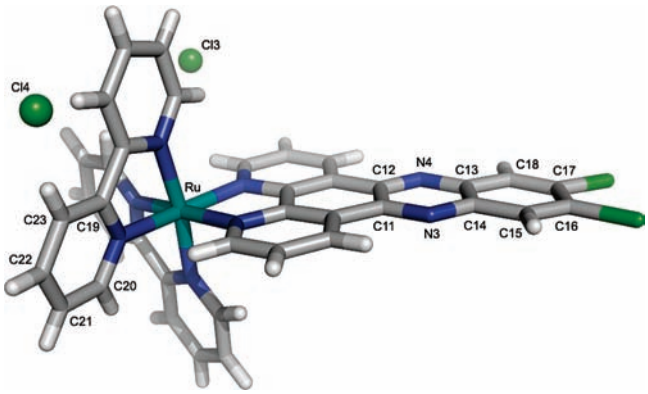

Figure 4. Molecular structure of $[Ru(bipy)_2(dppz(Cl_2))]Cl_2$.

purify $[Ru(bipy)_2\mathbf{L_I}]Cl_2$ and $[Ru(bipy)_2\mathbf{L_{II}}]Cl_2$ using normal phased column chromatography (these chloride complexes are too heavily adsorbed on alumina or silica). It should be mentioned that such chloride complexes can be purified using size-exclusion chromatography.[52] Pure $[Ru(bipy)_2\mathbf{L_I}]Cl_2$ and $[Ru(bipy)_2\mathbf{L_{II}}]Cl_2$ were prepared by a metathesis reaction between pure $[Ru(bipy)_2\mathbf{L_I}](PF_6)_2$ and $[Ru(bipy)_2\mathbf{L_{II}}](PF_6)_2$, respectively, and lithium chloride. $[Ru(bipy)_2\mathbf{L_I}](NTf_2)_2$ and $[Ru(bipy)_2\mathbf{L_{II}}](NTf_2)_2$ were synthesized by a metathesis reaction between $[Ru(bipy)_2\mathbf{L_I}]Cl_2$ and $[Ru(bipy)_2\mathbf{L_{II}}]Cl_2$, respectively, and lithium bis(trifluoromethylsulfonyl)imide ($LiNTf_2$; note that bis(trifluoromethylsulfonyl)imide and bistriflimide are synonyms).

Single Crystal X-ray Diffraction. Unfortunately, no single crystals could be obtained of the mesomorphic ruthenium(II) complexes. The long alkyl chains most probably prevent crystallization. However, suitable crystals of $[Ru(bipy)_2(dppz(Cl_2))]Cl_2$ (dppz: dipyrido phenazine) were obtained by slow evaporation of a solution of the complex in ethanol. The compound crystallized in the centrosymmetric space group $P2_1/c$; hence, both enantiomers are present in the crystal structure.

The asymmetrical unit of $[Ru(bipy)_2(dppz(Cl_2))]Cl_2 \cdot (H_2O)_4 \cdot (C_2H_5OH)$ consists of a $[Ru(bipy)_2(dppz(Cl_2))]^{2+}$ cation, two chloride anions, four water molecules, and one ethanol solvent molecule. The molecular structure of $[Ru(bipy)_2(dppz(Cl_2))]Cl_2$ is shown in Figure 4. The two bipyridine ligands and the dipyrido phenazine ligand are each bidentately coordinating to the ruthenium(II) cation. The geometry around ruthenium(II) can be described as a distorted octahedron. The Ru−N distances range from 2.051(3) to 2.076(3) Å; the coordination angles deviate from an ideal octahedron and range from 78.5(1)° to 97.7(1)°. The two bipyridine ligands are almost planar with dihedral angles ranging from 3.5(2)° to 10.3(2)°.

In the packing of the crystal structure (Figure 5), π-π stacking interactions can be observed between the phenazine ligand and the same phenazine ligand of a neighboring symmetry equivalent molecule, in particular between the rings C13−C18 and N3,N4,C11−C14 (centroid distance of 3.521(2) Å). Additional π-π interactions are found between

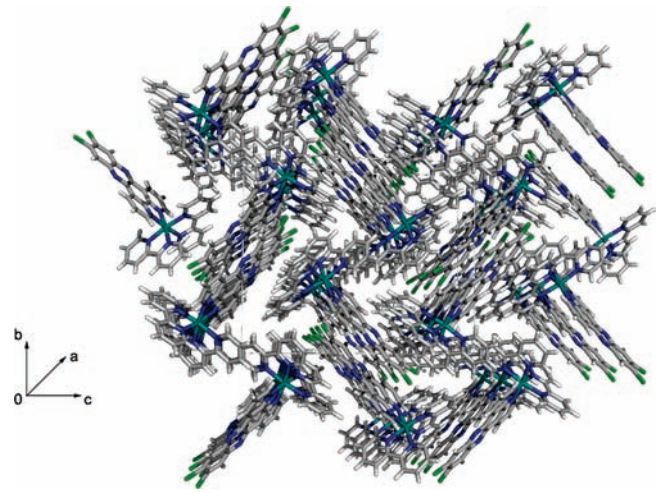

Figure 5. Packing in the crystal structure of $[Ru(bipy)_2(dppz(Cl_2))]Cl_2 \cdot (H_2O)_4 \cdot (C_2H_5OH)$. The chloride anions, and the water and solvent molecules are omitted for clarity.

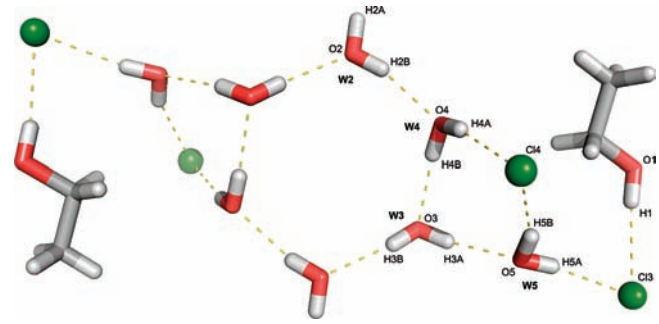

Figure 6. Network of hydrogen bonds in the crystal structure of $[Ru(bipy)_2(dppz(Cl_2))]Cl_2 \cdot (H_2O)_4 \cdot (C_2H_5OH)$. The atom labeling is only given for one asymmetric unit.

the phenazine ring C13−C18 and the bipyridine ring C19−C23 (centroid distance of 3.499(2) Å).

An intermolecular network of hydrogen bridges between the chloride anions and the water and ethanol solvent molecules is observed. The ethanol molecule forms a hydrogen bond with the Cl3-anion (O1−H1···Cl3 distance is 2.38(4) Å). This Cl3-anion is connected via water molecule W5 to the second Cl4 anion (O5−H5A···Cl3 distance is 3.35(4) Å and the O5−H5B···Cl4 distance is 2.42(4) Å). This water molecule W5 is connected via hydrogen bonds to a next water molecule W3 (O3−H3A···O5 distance is 1.96(4) Å). The water molecules W3, W4, and W2, respectively, are connected via hydrogen bonds (O2−H2B···O4 distance is 2.03(4) Å, the O4−H4B···O3 distance is 2.01(4) Å, and the O3−H3B···O2′ distance is 2.05(4) Å), which results in a hexagon of hydrogen bound water molecules with an inversion center in the middle (Figure 6).

Thermal Behavior. The ligands $\mathbf{L_I}$, $\mathbf{L_{II}}$, and the rhenium(I) complex $[ReBr(CO)_3\mathbf{L_{II}}]$ were not liquid-crystalline and melted to the isotropic liquid at 116, 119, and 205 °C, respectively. The thermal properties of all the ruthenium(II) complexes were examined by polarizing optical microscopy (POM), differential scanning calorimetry (DSC), and for some of them by X-ray diffraction on powder samples (vide infra). The thermal data for all the ruthenium(II) complexes

(52) Seddon, K. R.; Yousif, Y. Z. *Transition Met. Chem.* **1986**, *11*, 443–446.

Table 1. Thermal Data for the Ruthenium(II) Complexes

compound	thermal behavior[a,b]
$[Ru(bipy)_2\mathbf{L_I}]Cl_2$	Cr 227 SmA dec ~ 250
$[Ru(bipy)_2\mathbf{L_{II}}]Cl_2$	Cr 197 SmA dec ~ 250
$[Ru(bipy)_2\mathbf{L_I}](PF_6)_2$	Cr 185 SmA dec ~ 300
$[Ru(bipy)_2\mathbf{L_{II}}](PF_6)_2$	Cr 173 SmA dec ~ 300
$[Ru(bipy)_2\mathbf{L_I}](NTf_2)_2$	Cr 76 SmA 188 I
$[Ru(bipy)_2\mathbf{L_{II}}](NTf_2)_2$	Cr 53 I

[a] Abbreviations: Cr = crystalline or partially crystalline phase; SmA = smectic A phase; I = isotropic liquid; dec = decomposition. [b] All the transition temperatures listed in this table are those observed by POM.

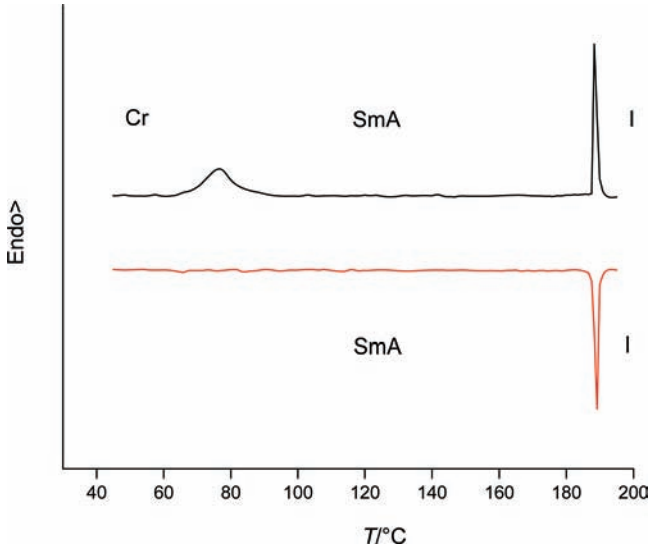

Figure 7. DSC trace of $[Ru(bipy)_2\mathbf{L_I}](NTf_2)_2$ (first heating/cooling run; heating/cooling rate of 10 °C min^{-1}). The heating run is shown in black whereas the cooling run is shown in red. Abbreviations: Cr = crystalline or partially crystalline phase; SmA = smectic A phase; I = isotropic liquid. Endothermic transitions are pointing upward (melting enthalpy $\Delta H_m = 0.9$ kJ mol^{-1}; clearing enthalpy $\Delta H_c = 0.6$ kJ mol^{-1}).

are collected in Table 1. A typical DSC trace of $[Ru(bipy)_2\mathbf{L_I}](NTf_2)_2$ is shown in Figure 7. Except for $[Ru(bipy)_2\mathbf{L_{II}}](NTf_2)_2$, all the ruthenium(II) complexes showed enantiotropic SmA phases, which were identified by their optical textures, observed by POM. The (fluid) SmA phases were recognized by the formation of bâtonnets on cooling from the isotropic liquid. On further cooling, an oily streak texture containing homeotropic domains (Figure 8 - top) or a focal conic texture (Figure 8 - bottom) was formed.

The observation of SmA phases could be expected. Indeed, lamellar mesophases are most commonly observed for ionic (metal-containing) liquid crystals.[24] The strong, isotropic electrostatic forces between neighboring ruthenium(II) complexes and their counterions stabilize a lamellar arrangement.

The lack of mesomorphism observed for $[Ru(bipy)_2\mathbf{L_{II}}](NTf_2)_2$ was very surprising because the analogous bistriflimide complex $[Ru(bipy)_2\mathbf{L_I}](NTf_2)_2$ did show a smectic A phase. In addition, the transition temperatures of the ruthenium(II) complexes containing the same counterions are similar (although slightly lower for the ruthenium(II) complexes of $\mathbf{L_{II}}$). A possible reason for this is that in the case of $[Ru(bipy)_2\mathbf{L_{II}}](NTf_2)_2$, $\mathbf{L_{II}}$ is rigid and cannot form any hydrogen bonds with neighboring ruthenium(II) complexes. On the contrary, in the case of $[Ru(bipy)_2\mathbf{L_I}](NTf_2)_2$, $\mathbf{L_I}$ is flexible (because of the single bond between the imidazole ring and the terminal phenyl ring) and can form hydrogen

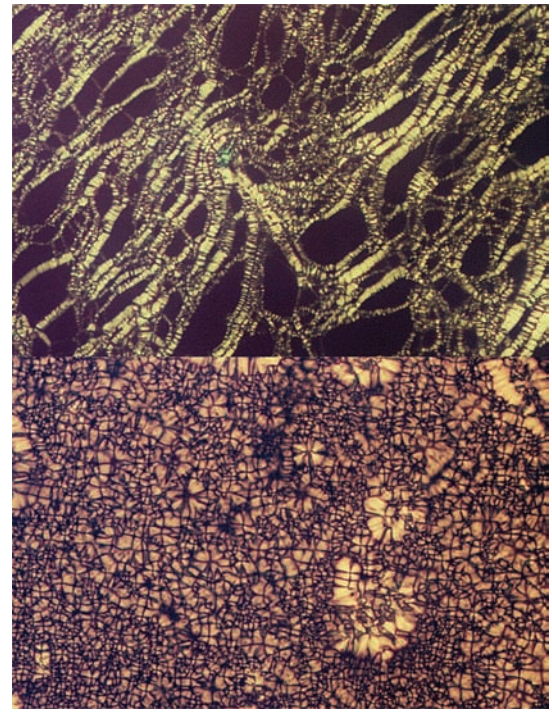

Figure 8. Top: oily streak texture of the SmA phase of $[Ru(bipy)_2\mathbf{L_I}](NTf_2)_2$ at 178 °C (200× magnification). Bottom: focal conic texture of the SmA phase of $[Ru(bipy)_2\mathbf{L_I}](NTf_2)_2$ at 165 °C (200× magnification).

bonds with neighboring ruthenium(II) complexes via the N−H group of the imidazole ring. Indeed, in the crystal structure of a ligand analogous to $\mathbf{L_I}$ (containing one hexyloxy chain instead of two octadecyloxy chains), it is clear that these ligands form strong hydrogen bonds.[31] In addition, $[Ru(bipy)_2\mathbf{L_I}](NTf_2)_2$ was investigated by infrared spectroscopy. The N−H stretching vibration, ν(N−H), was observed as a broad signal at 3319 cm^{-1}, indicating hydrogen bonding. Indeed, matrix-isolation FT-IR studies of benzimidazoles showed that the N−H stretching vibration of non-hydrogen-bonded benzimidazoles is observed at approximately 3500 cm^{-1}.[53] Possible hydrogen acceptors are the nitrogen atom of the imidazole ring, the negatively charged nitrogen atom of the bistriflimide anions (which is the strongest acceptor because of the negative charge), or the oxygen atoms of the bistriflimide anions. Thus, for $[Ru(bipy)_2\mathbf{L_{II}}](NTf_2)_2$, we assume that the large bistriflimide anions may disrupt the (π-π) interactions, and as a consequence, the self-assembly into a lamellar phase is inhibited. On the other hand, for $[Ru(bipy)_2\mathbf{L_I}](NTf_2)_2$, the strong hydrogen bonding interactions preserve the formation of a lamellar phase.

The influence of the type of counterion (PF_6^-, Cl^-, and NTf_2^-) is large. The highest transition temperatures were observed for the ruthenium(II) complexes containing (small) chloride anions ($[Ru(bipy)_2\mathbf{L_I}]Cl_2$ and $[Ru(bipy)_2\mathbf{L_{II}}]Cl_2$) whereas the lowest transition temperatures were observed for the ruthenium(II) complexes containing (large) bistriflimide anions ($[Ru(bipy)_2\mathbf{L_I}](NTf_2)_2$ and $[Ru(bipy)_2\mathbf{L_{II}}](NTf_2)_2$). Introduction of bistriflimide anions lowered the

(53) Schoone, K.; Smets, J.; Houben, L.; Van Bael, M. K.; Adamowicz, L.; Maes, G. *J. Phys. Chem. A* **1998**, *102*, 4863–4877.

Table 2. Bragg Reflections Collected from the SAXS Patterns of All the Mesomorphic Ruthenium(II) Complexes

compds	T/°C	d_{exp}/Å[a]	[hkl][b]	I[c]	d_{theo}/Å[a,d]	parameters[d]
[Ru(bipy)$_2$**L$_I$**](PF$_6$)$_2$	200	52.38	001	VS (sh)	52.52	SmA
		17.55	003	W (sh)	17.51	d = 52.52 Å
						V_{mol} = 2885 Å^3
						A_M = 109.86 Å^2
						A_{CH} = 27.47 Å^2
[Ru(bipy)$_2$**L$_{II}$**](PF$_6$)$_2$	200	46.72	001	VS (sh)	46.79	SmA
		23.36	002	W (sh)	23.39	d = 46.79 Å
		15.64	003	W (sh)	15.60	V_{mol} = 2919 Å^3
						A_M = 124.77 Å^2
						A_{CH} = 31.19 Å^2
[Ru(bipy)$_2$**L$_I$**]Cl$_2$	240	53.60	001	VS (sh)	53.61	SmA
		17.87	003	W (sh)	17.87	d = 53.61 Å
						V_{mol} = 2540 Å^3
						A_M = 94.76 Å^2
						A_{CH} = 23.69 Å^2
[Ru(bipy)$_2$**L$_{II}$**]Cl$_2$	240	49.39	001	VS (sh)	49.39	SmA
		16.46	003	W (sh)	16.46	d = 49.39 Å
						V_{mol} = 2575 Å^3
						A_M = 104.27 Å^2
						A_{CH} = 26.07 Å^2
[Ru(bipy)$_2$**L$_I$**](NTf$_2$)$_2$	140	50.84	001	VS (sh)	51.05	SmA
		25.61	002	W (sh)	25.53	d = 51.05 Å
		17.03	003	W (sh)	17.02	V_{mol} = 3259 Å^3
						A_M = 127.68 Å^2
						A_{CH} = 31.92 Å^2

[a] d_{exp} and d_{theo} are the experimentally measured and theoretical diffraction spacings. The distances are given in angstrom. [b] [hkl] are the Miller indices of the reflections. [c] Intensity of the reflections: VS: very strong, W: weak; sh stands for sharp reflections. [d] d_{theo} and the mesophases parameters d and A_M are deduced from the following mathematical expressions: $d = \langle d_{001} \rangle = [\sum_l d_{00l}.l]/N_{00l}$ where N_{00l} is the number of $00l$ reflections, the ionic headgroup area $A_M = 2V_{mol}/d$ and $A_{CH} = A_M/4$. V_{mol} is the molecular volume: $V_{mol} = M/0.6022\rho$, where $\rho = 27.0673/V_{CH2}$ and M is the molecular weight (g mol^{-1}) ($V_{CH2} = 26.5616 + 0.02023T$ (T in °C)). Abbreviations: SmA = smectic A phase.

transition temperatures by more than 100 °C! [Ru(bipy)$_2$-**L$_I$**](NTf$_2$)$_2$ and [Ru(bipy)$_2$**L$_{II}$**](NTf$_2$)$_2$ melted below 100 °C and consequently can be considered as ionic liquids. Except for [Ru(bipy)$_2$**L$_I$**](NTf$_2$)$_2$, all the mesomorphic ruthenium(II) complexes decompose before reaching the clearing point (T_{dec} > 200 °C) and the chloride complexes ([Ru(bipy)$_2$**L$_I$**]Cl$_2$ and [Ru(bipy)$_2$**L$_{II}$**]Cl$_2$) were thermally less stable than the hexafluorophosphate complexes ([Ru(bipy)$_2$**L$_I$**](PF$_6$)$_2$ and [Ru(bipy)$_2$**L$_{II}$**](PF$_6$)$_2$).

Small-Angle X-ray Scattering. All the mesomorphic ruthenium(II) complexes were studied by small-angle X-ray scattering (SAXS) using synchrotron radiation on powder samples. The ruthenium(II) complexes decompose fast when they are exposed to X-rays at high temperatures, and thus synchrotron radiation was needed since laboratory sources are too weak to yield interpretable scattering patterns in short time frames. The data collected from the SAXS patterns are presented in Table 2. The nature of the smectic A phases of [Ru(bipy)$_2$**L$_I$**](PF$_6$)$_2$, [Ru(bipy)$_2$**L$_{II}$**](PF$_6$)$_2$, [Ru(bipy)$_2$**L$_I$**]Cl$_2$, [Ru(bipy)$_2$**L$_{II}$**]Cl$_2$, and [Ru(bipy)$_2$**L$_I$**](NTf$_2$)$_2$ was confirmed by SAXS. SAXS patterns typical for smectic phases were recorded (Figure 9 shows a typical SAXS pattern of [Ru(bipy)$_2$**L$_I$**](NTf$_2$)$_2$). Several sharp reflections in the reciprocal spacing ratio 1:2:3 or 1:3 were observed (Table 2), corresponding to the lamellar periodicity (layer thickness) d = 52.52 Å, 46.79 Å, 53.61 Å, 49.39 Å, and 51.05 Å for Ru(bipy)$_2$**L$_I$**](PF$_6$)$_2$, [Ru(bipy)$_2$**L$_{II}$**](PF$_6$)$_2$, [Ru(bipy)$_2$**L$_I$**]Cl$_2$, [Ru(bipy)$_2$**L$_{II}$**]Cl$_2$, and [Ru(bipy)$_2$**L$_I$**](NTf$_2$)$_2$, respectively.

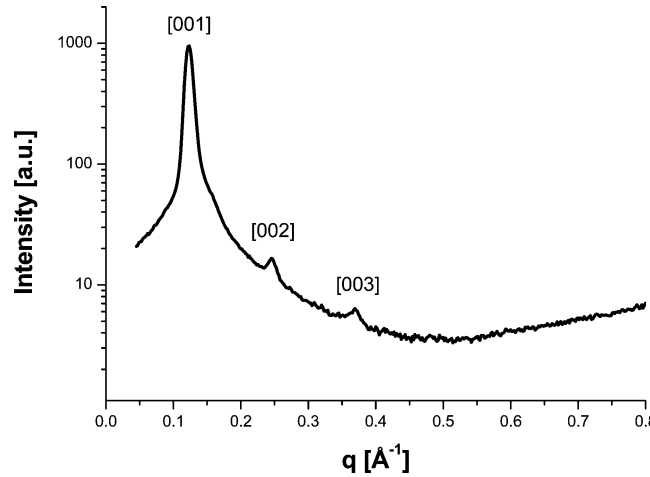

Figure 9. SAXS pattern of [Ru(bipy)$_2$**L$_I$**](NTf$_2$)$_2$ at 140 °C. [hkl] are the Miller indices of the reflections.

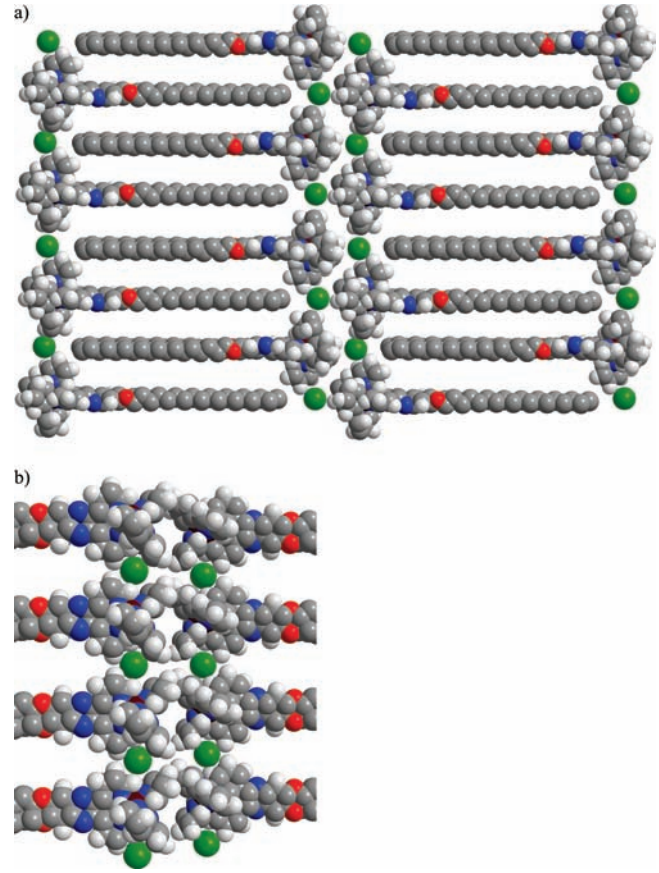

Figure 10. (a) Spacefilling model representing the molecular arrangement in the SmA phase of the mesomorphic ruthenium(II) complex [Ru(bipy)$_2$**L$_{II}$**]Cl$_2$. (b) Orthogonal view of the ionic layer portion of the spacefilling model. For each viewpoint, only one out of two counterions of each ruthenium compound is shown for the sake of clarity.

The relative intensities of these reflections depend on the internal (electron density) structure of the stacked layers.

All the mesomorphic ruthenium(II) complexes show a similar molecular organization. A molecular model that shows the organization of [Ru(bipy)$_2$**L$_{II}$**]Cl$_2$ complexes in the SmA layers is proposed in Figure 10. The molecules are arranged head-to-head, leading to a microphase separation between ionic parts and aliphatic chains. In this way, the area of an ionic headgroup $A_M = 2V_{mol}/d$ is found to be

95−128 Å^2 (V_{mol} is calculated using the relation $V_{mol} = (M/0.6022)f$, where M is the molecular mass (g mol^{-1}) and f is a temperature correcting factor ($f = 0.9813 + 7.474 \times 10^{-4}T$; T in °C). Such a large headgroup area is counterbalanced by four aliphatic chains, resulting in a molecular cross-sectional area per aliphatic chain of $A_{CH} = A_M/4 = 24-32$ Å^2. This is achieved by an almost complete interdigitation of the aliphatic chains, which is supported by the fact that d is only $1.2 \times L$ (L is the molecular length estimated by Chem3D). In addition, the Coulombic interactions demand a strict alternation of positive and negative charges, and this can only be achieved by placing the cations and anions as proposed by the molecular models represented in Figure 10.

Because the ruthenium(II) complexes are amphiphilic molecules (surfactant structure), analysis on the basis of packing constraints was run alongside.[54] The analysis is only given for [Ru(bipy)$_2$**L$_{II}$**]Cl$_2$ because all the mesomorphic ruthenium(II) complexes show a similar molecular organization within the mesophases. The critical parameter $V/A_M l$ (V is the volume of the aliphatic chains, A_M is the area of the ionic headgroup (vide supra), and l is the extended length of the aliphatic chains) can be calculated. As $V = 2(nV_{CH2} + V_{CH3})$, where 2 corresponds to the number of chains per ruthenium complex, n, the number of methylene groups per chain, V_{CH2}, the volume of one methylene unit ($V_{CH2} = 26.5616 + 0.02023T$, T the temperature in °C), and V_{CH3}, the volume contribution of the end group ($V_{CH3} = 27.14 + 0.01713T + 0.0004181T^2$), V is calculated to be 1178.84 Å^3.[55] A_M was calculated to be 104.27 Å^2 (see Table 2) and l was estimated by Chem3D to be 22.57 Å. Thus, the parameter $V/A_M l$ is found to be 0.5. However, for a lamellar arrangement, $V/A_M l$ should be approximately 1. Therefore, the aliphatic chains must be completely interdigitating: this theoretically means four aliphatic chains per ruthenium(II) complex. In this case, $V = 4(nV_{CH2} + V_{CH3}) = 2357.68$ Å^3 and using the same values for A_M and l, the parameter $V/A_M l = 1$, which is perfectly in agreement with a lamellar arrangement. Thus, the packing constraint analysis confirms the molecular model proposed in Figure 10.

The area of the ionic headgroups depends on the size of the anions but also on the ligand type. When comparing [Ru(bipy)$_2$**L$_I$**]Cl$_2$ and [Ru(bipy)$_2$**L$_I$**](NTf$_2$)$_2$, the area of the ionic headgroup of [Ru(bipy)$_2$**L$_I$**]Cl$_2$ (A_M = 94.76 Å^2) is much smaller than that of [Ru(bipy)$_2$**L$_I$**](NTf$_2$)$_2$ (A_M = 127.68 Å^2). The larger headgroup area in the case of [Ru(bipy)$_2$**L$_I$**](NTf$_2$)$_2$ (caused by the larger NTf$_2^-$ ions) is counterbalanced by folding of the aliphatic chains: A_{CH} = 31.92 Å^2 for [Ru(bipy)$_2$**L$_I$**](NTf$_2$)$_2$ while A_{CH} = 23.69 Å^2 for [Ru(bipy)$_2$**L$_I$**]Cl$_2$. Consequently, the layer spacing in the case of [Ru(bipy)$_2$**L$_I$**]Cl$_2$ is larger (d = 53.61 Å) than the layer spacing in the case of [Ru(bipy)$_2$**L$_I$**](NTf$_2$)$_2$ (d = 51.05 Å). It should be noted that the observed layer spacings are measured at different temperatures (at 240 °C for [Ru(bipy)$_2$**L$_I$**]Cl$_2$ and at 140 °C for [Ru(bipy)$_2$**L$_I$**](NTf$_2$)$_2$, see Table 2) and the layer spacing decreases with increasing length of the aliphatic chains for SmA phases (because of a higher degree of disorganization of the aliphatic chains at higher temperatures). This means that the layer spacing of [Ru(bipy)$_2$**L$_I$**](NTf$_2$)$_2$ would be even smaller at 240 °C. When comparing [Ru(bipy)$_2$**L$_I$**](PF$_6$)$_2$ and [Ru(bipy)$_2$**L$_{II}$**](PF$_6$)$_2$, the area of the ionic heagroup of [Ru(bipy)$_2$**L$_I$**](PF$_6$)$_2$ (A_M = 109.86 Å^2) is smaller than that of [Ru(bipy)$_2$**L$_{II}$**](PF$_6$)$_2$ (A_M = 124.77 Å^2). Again, the larger headgroup area in the case of [Ru(bipy)$_2$**L$_{II}$**](PF$_6$)$_2$ (caused by the different molecular structure of **L$_{II}$**) is counterbalanced by folding of the aliphatic chains: A_{CH} = 31.19 Å^2 and d = 46.79 Å for [Ru(bipy)$_2$-**L$_{II}$**](PF$_6$)$_2$, while A_{CH} = 27.47 Å^2 and d = 52.52 Å for [Ru(bipy)$_2$**L$_I$**](PF$_6$)$_2$. It should be noted that the rigid part of **L$_{II}$** is slightly smaller than that of **L$_I$** (Δl_{core} = 1.6 Å, estimated by Chem3D), which should also be taken into account to explain the smaller layer thickness in the case of ruthenium(II) complexes of **L$_{II}$**. Indeed, as the critical parameter $A_M = V/l$ for lamellar phases (A_M = 109.86 Å^2 and 124.77 Å^2 for [Ru(bipy)$_2$**L$_I$**](PF$_6$)$_2$ and [Ru(bipy)$_2$**L$_{II}$**]-(PF$_6$)$_2$, respectively; V can be calculated to be 2270.48 Å^3 at 200 °C), l can be calculated to be 20.66 Å and 18.20 Å for [Ru(bipy)$_2$**L$_I$**](PF$_6$)$_2$ and [Ru(bipy)$_2$**L$_{II}$**](PF$_6$)$_2$, respectively. Thus the difference in the length of the aliphatic chains, Δl_{chain} = 2.46 Å, and the total difference in layer spacing, $\Delta d = \Delta l_{chain} + 2\Delta l_{core}$ = 5.66 Å. This value is in good agreement with the measured difference in layer spacing (52.52 Å − 46.79 Å = 5.73 Å).

Photophysical Properties. Ruthenium(II) polypyridine complexes are well-known and well studied complexes with a d^6 octahedral strong crystal field configuration. They are chemically stable, have interesting luminescence properties, and these compounds have attracted a lot of attention for applications as DNA-intercalating luminescent probe and photoenergy conversion.[56,57] Their absorption spectrum is characterized by several intense bands. The absorption spectra of both the [Ru(bipy)$_2$**L$_I$**]$^{2+}$ and [Ru(bipy)$_2$**L$_{II}$**]$^{2+}$ compounds in chloroform are presented in Figure 11. The lowest-energy absorption band around 450 nm can be attributed to a metal-to-ligand charge-transfer (MLCT) transition $\pi^* \leftarrow d_\pi$(Ru). The intense intraligand band around 275 nm originates from a bipyridine $\pi^* \leftarrow \pi$ transition. The smaller bands around 330 nm are attributed to intraligand bands from the **L$_I$** or **L$_{II}$** ligands. Metal centered d-d transitions are forbidden by the Laporte selection rules, and because of their low intensity, they are buried under the MCLT bands. Absorption and luminescence spectra of similar complexes without the long alkyl chains were already recorded in other solvents for both **L$_I$** and **L$_{II}$**.[58,59]

In chloroform, the excitation of the MLCT transition around 450 nm results in a typical emission around 610 nm,

(54) Israelachvili, J. N.; Mitchell, D. J.; Ninham, B. W. *J. Chem. Soc., Faraday Trans.* **1976**, *72*, 1525–1568.
(55) Donnio, B.; Heinrich, B.; Allouchi, H.; Kain, J.; Diele, S.; Guillon, D.; Bruce, D. W. *J. Am. Chem. Soc.* **2004**, *126*, 15258–15268.
(56) Friedman, A. E.; Chambron, J. C.; Sauvage, J. P.; Turro, N. J.; Barton, J. K. *J. Am. Chem. Soc.* **1990**, *112*, 4960–4962.
(57) Juris, A.; Balzani, V.; Barigelletti, F.; Campagna, S.; Belser, P.; Vonzelewsky, A. *Coord. Chem. Rev.* **1988**, *84*, 85–277.
(58) Albano, G.; Belser, P.; De Cola, L.; Gandolfi, M. T. *Chem. Commun.* **1999**, 1171–1172.
(59) Jing, B. W.; Zhang, M. H.; Shen, T. *Spectrochim. Acta, Part A* **2004**, *60*, 2635–2641.

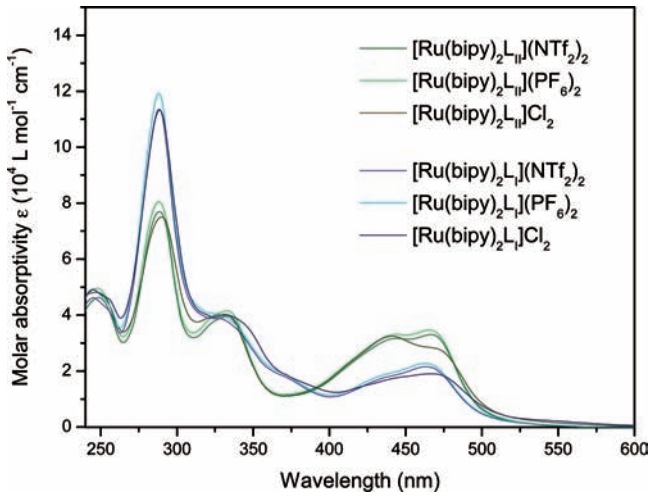

Figure 11. Absorption spectrum of $[Ru(bipy)_2\mathbf{L_I}]^{2+}$ and $[Ru(bipy)_2\mathbf{L_{II}}]^{2+}$ in chloroform.

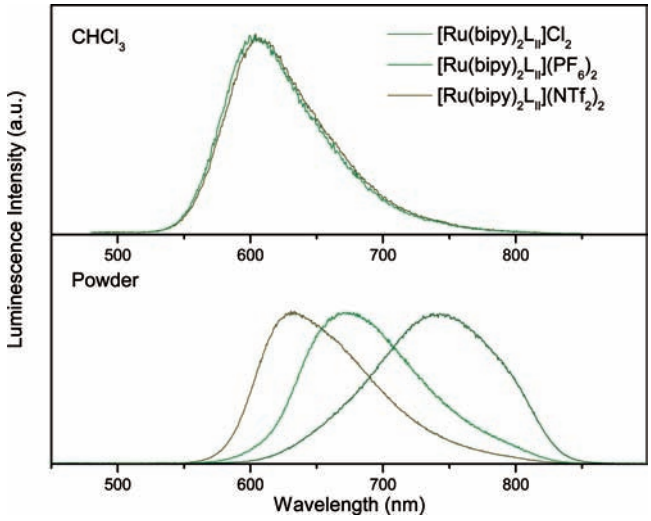

Figure 12. Luminescence spectrum of $[Ru(bipy)_2\mathbf{L_{II}}]Cl_2$, $[Ru(bipy)_2\mathbf{L_{II}}](PF_6)_2$, and $[Ru(bipy)_2\mathbf{L_{II}}](NTf_2)_2$. Excitation wavelength is 450 nm for the chloroform solutions and 400 nm for the powders.

which is the same for the $\mathbf{L_I}$ and $\mathbf{L_{II}}$ ligands with different anions. The luminescence spectra for $[Ru(bipy)_2\mathbf{L_{II}}]^{2+}$ in chloroform and for the pure powders are presented in Figure 12. The luminescence maximum of the $[Ru(bipy)_2\mathbf{L_I}]^{2+}$ powders is situated at 630 nm and does not depend on the anion. On the contrary, the $[Ru(bipy)_2\mathbf{L_{II}}]^{2+}$ luminescence maximum shifts from 630 to 670 nm and 740 nm for NTf_2^-, PF_6^-, and Cl^- anions, respectively (Figure 12). In the solid state of compounds with a large conjugated system (which thus consist of a large number of aromatic units), the π-π interactions are of prime importance. The π-π interactions of the pyrazino[2,3-f]-1,10-phenanthroline play an important role in the binding of similar ruthenium(II) complexes with DNA.[56] Indeed, the presence of strong π-π interactions between the pyrazino[2,3-f]-1,10-phenanthroline units was confirmed by single crystal structure studies (vide supra). If the packing, and therefore the interactions for the more extended, aromatic pyrazino[2,3-f]-1,10-phenanthroline ring differ in the case of different anions, this would induce a shift in the sensitive charge transfer levels and consequently alters its luminescence spectrum. On the other hand, for $[Ru(bipy)_2\mathbf{L_I}]^{2+}$, the luminescence maximum is not affected by the type of anion. This indicates that the packing within the solid state is similar for different anions. This is probably due to the fact that the strong hydrogen bonding interactions between the imidazo[4,5-f]-1,10-phenanthroline units are dominant in the case of $[Ru(bipy)_2\mathbf{L_I}]^{2+}$ (vide supra). The striking difference in thermal behavior between $[Ru(bipy)_2\mathbf{L_I}](NTf_2)_2$ and $[Ru(bipy)_2\mathbf{L_{II}}](NTf_2)_2$ also points to the fact that the intermolecular interactions for $\mathbf{L_I}$ and $\mathbf{L_{II}}$, respectively, are different (vide supra).

Conclusions

This paper shows that electrostatic interactions induce mesomorphism in high-coordination number metallomesogens. This is illustrated for imidazo[4,5-f]-1,10-phenanthroline and pyrazino[2,3-f]-1,10-phenanthroline ligands, which do not exhibit liquid-crystalline phases themselves. Complex formation of these ligands with the $[Re(CO)_3Br]$ unit does not lead to liquid-crystalline metal complexes. However, the ionic ruthenium(II) complexes are liquid-crystalline, and the transitions temperatures strongly depend on the counteranions. In all cases, a smectic A phase was observed. The ruthenium(II)-containing metallomesogens are highly luminescent and form a new class of luminescent liquid crystals. For the ruthenium(II) complexes of the pyrazino[2,3-f]-1,10-phenanthroline ligand, the luminescence color can be tuned by the choice of anion.

Acknowledgment. T.C. and K.D. thank the FWO-Flanders for a postdoctoral fellowship. K.B. thanks the K.U.Leuven (projects GOA 08/05 and IDO/05/005) and the FWO-Flanders (project G.0508.07). CHN analyses and mass spectra were obtained by Dirk Henot. The authors thank the technical staff of the DUBBLE beamline at the ESRF (Grenoble, France) for their assistance to the synchrotron measurements.

Supporting Information Available: CIF-files of the crystal structures. This material is available free of charge via the Internet at http://pubs.acs.org.

IC801772Q